Three-component zipper assembly of photoactive cascade architectures with blue, red and colorless naphthalenediimide donors and acceptors†

Naomi Sakai, Ravuri S. K. Kishore and Stefan Matile*

Received 16th May 2008, Accepted 5th August 2008
First published as an Advance Article on the web 10th September 2008
DOI: 10.1039/b808288j

We report the programmed ("zipper") assembly of photoactive rigid-rod π-stack architectures composed of blue (b), red (r) and colorless (n) core-substituted naphthalene diimides (NDIs) attached along *p*-oligophenyl (POP) rods. The design strategy and multistep syntheses of the required NDI–POP conjugates are described first. The activity of the obtained up to three-component cascade architectures is characterized in current–voltage curves, which are analyzed to reveal short circuit currents and fill factors as significant characteristics. With one-component zippers, rNDIs are found to give much higher photocurrents than bNDIs. In two-component zippers, substitution of rNDIs by nNDIs in meaningful positions is shown to give increased photocurrents despite reduced absorption of light. Three-component zippers are shown to provide access to an increased structural complexity for more subtle control of function. Reaching from 0.27 to 0.54, fill factors, a measure for the power generated with light, are found to be most sensitive to the directionality of multicomponent cascade architectures. Overall, these results are in agreement with photoinduced charge separation between rNDI (but not bNDI) acceptors and POP donors followed by directional intrastack electron transfer from rNDI radical anions to nNDI acceptors, that is, the formation of supramolecular cascade *n*/*p*-heterojunctions.

Introduction

For future breakthroughs in advanced functional materials such as organic optoelectronics, it is essential to develop new strategies to build organic nanoarchitectures on surfaces with high accuracy.[1–30] This is difficult because it requires molecular-level control over vectorial organization in three dimensions (3D). Currently, many top-down methods are available to deposit bulk organic material as thin films on solid surfaces (vapor deposition, inkjet printing, sol-gel processes, roller casting, spin coating, *etc.*). Bulk deposition of an *n*-semiconductor and a *p*-semiconductor produces bulk *n*/*p*-heterojunctions, the central unit of most current organic solar cells.[5] Several examples for bulk deposition of vectorial multicomponent systems[6,7] and materials with supramolecular 1D (fibers,[8] nanotubes[9]) and 3D organization (mixed single crystals[10]) exist as well. However, bulk deposition methods are in general incompatible with rational control of the intrafilm molecular organization as well as the orientation of the molecules relative to the surfaces.

Approaches toward artificial photosystems with refined supramolecular architectures on solid substrates have been developed with respect to organization in one, two, and three dimensions. Highlights with regard to 1D organization include pioneering approaches toward supramolecular *n*/*p*-heterojunctions[8,9] and vectorial cascade systems (tobacco mosaic virus, dye-loaded zeolite channels).[11,12] Current interest concerning supramolecular 2D organization focuses on self-assembled monolayers (SAMs)[13,14] made from vectorial scaffolds such as peptides,[15] proteins[16] and DNAs,[17] as well as on two-component SAMs.[18,19] Layer-by-layer (LBL) deposition of polyelectrolytes from solution is the classical approach toward vectorial multicomponent photosystems with some ("fuzzy")[20] 3D organization.[20–26]

Approaches toward 3D organization beyond conventional electrostatic LBL are rather limited. The classical triple H-bonding motif with cyanurates and melamines was used in a study to extend the 2D organization in SAMs to 3D oligothiophene/fullerene architectures on the surface.[27] A spectacular approach to thick zinc porphyrin multilayers employed interlayer metal–ligand coordination followed by covalent cross-linking using Grubbs ring closing metathesis.[28] Vectorial architecture, finally, has been realized by combining copper and zirconium coordination chemistry to couple three porphyrin layers with three zinc porphyrin donor layers on gold and SiO_2.[29,30]

In general, these pioneering approaches toward advanced architectures[25–30] yielded photocurrents that correctly reflect expectations from the explored design strategy, whereas fill factors (*FF*) were, with one outstanding exception ($FF = 0.37–0.58$),[29] surprisingly low or not reported. In the few approaches beyond electrostatic LBL, the conceptual challenge of vectorial 3D organization on the supramolecular level is mostly neglected. To contribute toward this general objective, we have recently introduced zipper assembly (Fig. 1).[31,32] Initially, we have shown that one-component zipper assembly with blue naphthalene diimides (bNDIs) gives rise to higher photoactivity than the conventional LBL assembly, and responds to positive controls such as capping.[31] Later on, we have shown that zipper assembly with red NDIs (rNDIs) affords the photoinduced stack/rod charge separation needed for supramolecular *n*/*p*-heterojunctions, and that the directional electron transfer in two-component π-stacks with rNDIs and

Department of Organic Chemistry, University of Geneva, Geneva, Switzerland. E-mail: stefan.matile@chiorg.unige.ch; Fax: +41 22 379 5123; Tel: +41 22 379 6523

† Electronic supplementary information (ESI) available: Experimental details. See DOI: 10.1039/b808288j

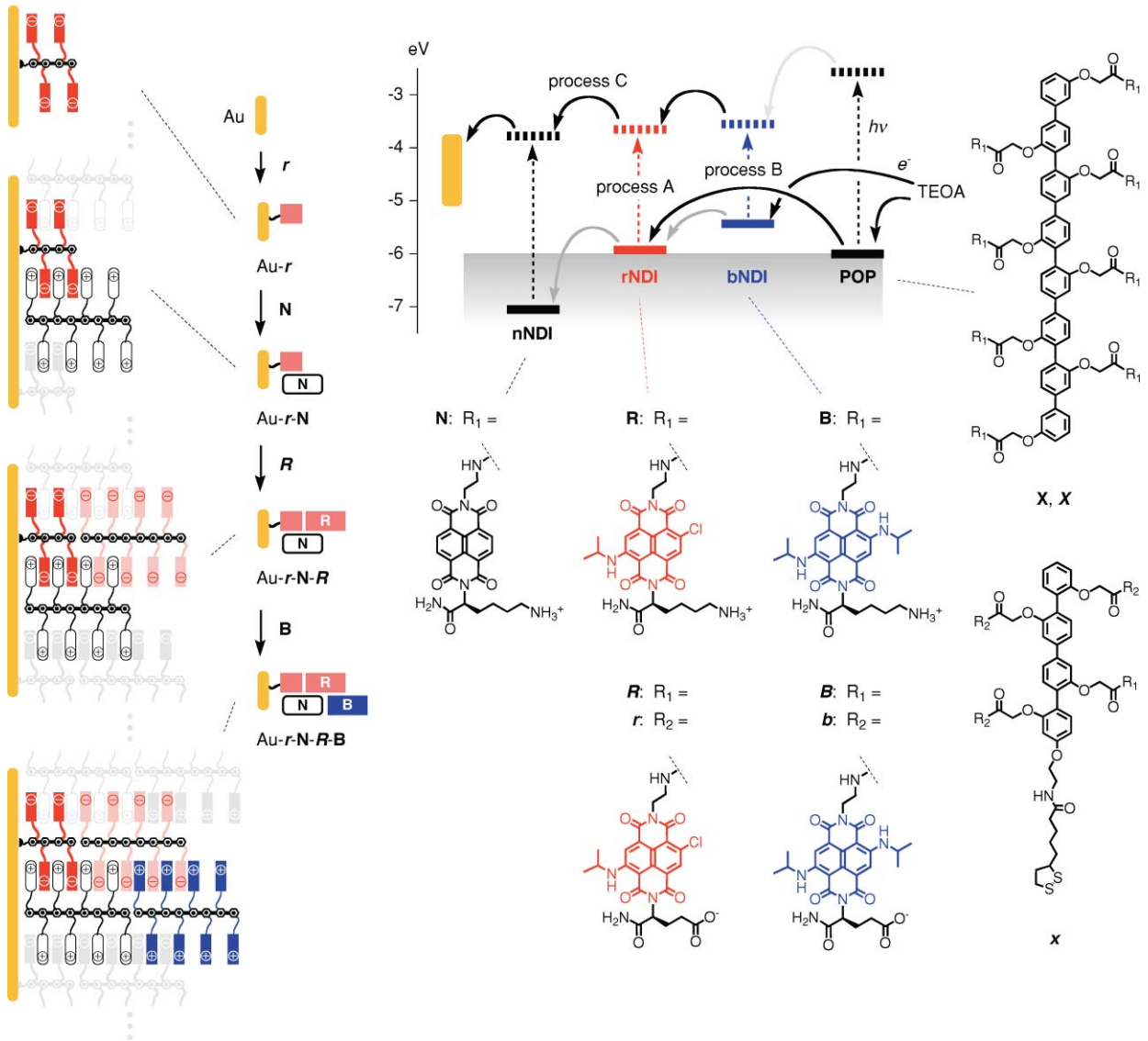

Fig. 1 Zipper assembly of vectorial cascade architectures composed of *n*-semiconducting π-stacks of blue (bNDI), red (rNDI) and colorless (nNDI) donors and acceptors along *p*-semiconducting *p*-oligophenyls (POPs) (*left*), molecular structures of initiators (***x*** = ***r***, ***b***) and cationic (**X** = **N**, **R**, **B**) and anionic (***X*** = ***R***, ***B***) propagators (for full structures, please see Fig. S1†), and frontier orbital energy levels (*right*). rNDIs in ***r***, **R**, and ***R*** are mixtures of 2,6- and 3,7-regioisomers, all suprastructures are speculative representations. Energy diagram: solid lines, HOMO; dashed lines, LUMO; solid arrows, electron transfer; dashed arrows, absorption of light (*hν*); black arrows, conceptually important electron transfer after excitation of rNDIs (process A) include photoinduced stack/rod charge separation (process B) and electron transfer within the cascade π-stack to the nNDI acceptor (process C).

bNDIs controls the fill factors in current–voltage relationships.[32] Here, we introduce three-component zippers, where bNDIs and rNDIs are combined with colorless nNDI electron acceptors in cascade π-stacks along POP rod donors. The position of these chromophores is systematically varied to explore the effect of cascading on the photoactivity of the resulting zippers.

Results and discussion

Design

Zipper assembly was conceived based on the earlier observation that the interdigitation of "unbendable" rigid-rod scaffolds is favorable and could lead to higher order supramolecular architectures.[33] This suggested that rigid-rod molecules with "sticky ends" could finally provide the interlayer recognition motif needed for supramolecular multicomponent vectorial 3D organization on solid substrates. We envisioned the π-stacking of interdigitating aromatics from adjacent, staggered rigid-rod scaffolds, oriented by hydrogen-bonded chains[35] as intralayer organization motifs. The electrostatic interactions between negative charges in ***r***, ***R***, ***b*** and ***B*** and the positive charges in **R**, **B** and **N** are expected not only to direct zipper assembly, but also to promote the interstack 2D organization (Fig. 1).[31]

For zipper assembly, *p*-oligophenyls (POPs) were selected as model rods[34–37] and naphthalenediimides (NDIs)[35–54] for model stacks. Zipper assembly requires at least three different components: here, initiators ***x*** (Fig. 1, ***x*** = ***b***, ***r***) consist of *p*-quaterphenyl

rods carrying a disulfide group at one terminus for covalent linkage to the gold surface and four anionic NDIs along the scaffold. Cationic propagators **X** are double-length *p*-octiphenyls with eight cationic NDIs attached along the scaffold (Fig. 1, **X** = **B**, **R**, **N**). One half of the cationic NDIs of propagators **X** are expected to form π-stacks with the anionic NDIs of initiators ***x*** to give zippers of the general structure Au-***x***-**X**. The free half of the cationic propagators **X** remain as "sticky ends" to zip up with one half of the anionic propagators ***X*** added next (Fig. 1, ***X*** = ***B***, ***R***). The resulting anionic sticky ends of zipper Au-***x***-**X**-***X*** can zip up with one half of cationic propagators **X** to give Au-***x***-**X**-***X***-**X**, and so on. The functional significance of sticky ends was supported by clear-cut inhibition of zipper assembly with *p*-quaterphenyl terminators ***x***.[31]

NDIs[35–54] were selected for zipper assembly because their spectroscopic and electrochemical properties can be extensively varied without global structural changes.[31,32,36,37,45–49] Moreover, their planarity and π-acidity[50,51] is ideal for the formation of *n*-semiconducting[40,41,44] face-to-face π-stacks next to strings of *p*-semiconducting[31,32] POP rods. In this study, three different NDIs are used. With π-donating alkylamines as core substituents, monomeric bNDIs are intensely blue (λ_{abs} 620 nm, ε 23 mM^{-1} cm^{-1}), red-fluorescent (λ_{em} 650 nm, Φ_{fl} 0.42) chromophores that can be both reduced (–1.3 V *vs.* Fc/Fc^{+}) and oxidized (+0.6 V).[36,37,46,47] The frontier energy levels calculated from these data (Fig. S2 and Table S1†) are shown in Fig. 1. Attached along *p*-octiphenyl scaffolds in **B**, bNDIs undergo quantitative, ultrafast (<2 ps) photoinduced charge separation (PCS) that lasts for 61 ps.[36] More recently, PCS with lifetime components up to 1 ns were identified in lipid bilayer membranes, where **B** self-assembles into tetrameric π-stack architectures.[54]

Replacement of one alkylamine with a chloride produces the red (λ_{abs} 535 nm, ε 16 mM^{-1} cm^{-1}), orange-fluorescent (λ_{em} 565 nm, Φ_{fl} 0.63) 2(3)-alkylamino-6(7)-chloro-1,4,5,8-NDI (rNDI) chromophore.[32] More electron-deficient, rNDIs are more easily reduced (–1.1 V) and more difficult to oxidize (+1.1 V, Fig. 1) than bNDIs. Quantitative ultrafast PCS of rNDIs attached along *p*-octiphenyl scaffolds in **R** lasts longer than 1 ns. Quenching experiments suggested that electron transfer from POP donors contributes to this long-lived PCS with **R** but not with **B** (Fig. 1, process B). Evidence for stack/rod PCS demonstrated that rNDIs but not bNDIs are compatible with the formation of a supramolecular *n*/*p*-heterojunction by zipper assembly. The action spectra of mixed zippers confirmed that photocurrent generation by rNDIs is much more efficient than with bNDIs.

Removal of both alkylamine core substituents gives the colorless, very weakly fluorescent nNDI (λ_{abs} 380 nm, ε 24 mM^{-1} cm^{-1}). Extensively studied for many diverse purposes,[35,37–43,50–53] nNDIs have a quadrupole moment $Q = +14.7$ B that is far beyond that of the best known π-acid, hexafluorobenzene, and thus ideal for π-stack architectures (preliminary computational data indicate that even bNDIs remain weakly π-acidic).[50] Importantly, nNDIs have an energetically deep-lying LUMO (–3.9 eV) that is near that of C_{60} (–4.2 eV), the most common acceptor in organic solar cells.[25] Electron withdrawing substituents such as cyano groups can be used to shift the electron affinity of NDIs beyond that of C_{60} without global structural changes.[45] As with C_{60}, a degenerate LUMO for multiple reversible reduction documents the ability to stabilize negative charges. FET charge mobilities of up to 0.12 $cm^2/(Vs)$ identified nNDIs as one of the few air stable and high-mobility n-channel organic semiconductors.[41,45]

In this study, nNDIs are introduced as electron acceptors in **N** for zipper assembly for up to three-component cascade NDI π-stacks. The energy levels of NDI chromophores suggest preferred electron transfer from bNDI to rNDI and then to nNDI (Fig. 1, process C).

Synthesis

The syntheses of initiator ***b*** and propagators ***B***, **R**, **B** and **N** have been described.[31,32,35,36] The anionic rNDI initiator ***r*** and propagator ***R*** were prepared analogously. The spectroscopic and analytical data of the new compounds were in agreement with their structure and homogeneity. Synthetic procedures and spectroscopic and analytical data can be found in the ESI.†

Red zippers

With the anionic rNDI initiator ***r*** and propagator ***R*** in hand, we first focused on the one-component assembly of red zippers. *p*-Quaterphenyl initiators ***r*** were deposited on gold electrodes following the procedure developed with the blue analogs ***b***.[31] The obtained Au-***r*** was dipped repeatedly into an aqueous solution of cationic and anionic *p*-octiphenyl propagators **R** and ***R***, respectively. Photocurrents were generated with triethanolamine (TEOA) as electron donor, the gold electrode below the red zippers as electron acceptor, the Pt electrode as cathode and Ag/AgCl as a reference. The photocurrents increased with increasing zipper assembly until Au-***r***-***R***-***R***-***R***-***R***-***R***-***R***-***R***-***R*** (Fig. 2, ○).

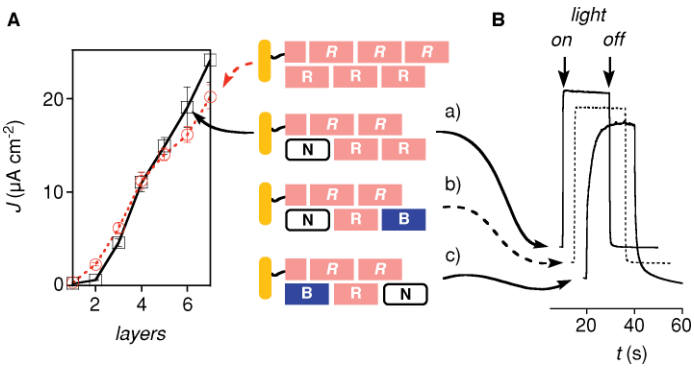

Fig. 2 (A) Dependence of photocurrent density at +0.4 V (*vs.* Ag/AgCl) on the number of layers of red rNDI zippers with (□, Au-***r***-N[-***R***-**R**]$_n$) or without (○, Au-***r***-**R**[-***R***-**R**]$_n$) an nNDI acceptor **N** at the beginning. (B) Intensity normalized kinetic data for photocurrent generation with light for (a) Au-***r***-N-***R***-**R**-***R***-**R**, (b) Au-***r***-N-***R***-**R**-***R***-**B**, and (c) Au-***r***-**B**-***R***-**R**-***R***-N.

Current–voltage (*IV*) relationships were measured for prepared zippers to identify the three values that determine the output power (*i.e.*, efficiency): the short circuit current density J_{SC}, the open circuit potential V_{OC} and the fill factor *FF* (Fig. 3). In general, J_{SC} is dictated by the incident photon to current conversion efficiency (IPCE), which is the product of light harvesting efficiency (LHE, *i.e.*, the concentration and absorption cross section of the used chromophores), quantum yield of charge injection and the charge collection efficiency at the back electrode. The open circuit potential V_{OC} is influenced by the bandgap between the HOMO of the relevant donor and the LUMO of the relevant acceptor.

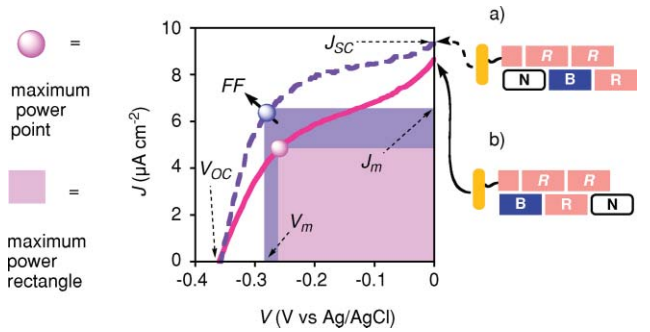

Fig. 3 Current–voltage profiles of three-component zippers Au-***r***-N-***R***-B-***R***-R (a) and Au-***r***-B-***R***-R-***R***-N (b) with indication of short circuit current density (J_{SC}), open circuit voltage (V_{OC}), maximum power rectangle and maximum power point, and fill factor FF = maximum power/$(V_{OC} \times J_{SC}) = (V_m \times J_m)/(V_{OC} \times J_{SC})$; compare Table 1, entries 9 and 16.

The fill factor (FF) is defined as maximum power/$(V_{OC} \times J_{SC})$, that is $FF = (V_m \times J_m)/(V_{OC} \times J_{SC})$ (Fig. 3). The electronic asymmetry of multicomponent cascade architectures is, among other parameters, expected to influence FF. All experiments were done at least twice, experimental errors were well within 10% (Fig. 2A), all important trends were reproducible.

The IV profiles of the red zippers revealed the comparably high photocurrents J_{SC} and fill factors FF expected for the long-lived stack/rod charge separation with the possible formation of supramolecular n/p-heterojunctions (Table 1, entries 1–3). The fill factors were constantly high and increased as more layers were assembled until an apparent saturation around $FF \sim 0.50$–0.54 was reached. To facilitate comparisons, we calculated relative FF, taking $FF = 0.25$ of linear I–V correlations and $FF = 0.61$ of optimized organic solar cells[1] as standard values (0 and 100%, respectively). The $FF = 0.49$–0.53 found for red zippers corresponded to a relative value of 67–78%. These excellent properties of the rNDIs turned out to hinder rather than help the evaluation of two- and three-component zippers because their powerful impact tended to obscure the more subtle contributions from nNDIs and bNDIs (see below).

Two-component zippers

The colorless nNDI acceptors of the cationic propagator **N** were added at the beginning of the red zippers to direct the flow of electrons in the envisioned two-component cascade NDI stacks toward the gold electrode (Fig. 1). Substitution of the second layer from cationic red propagators **R** to colorless propagators **N** resulted in reduced photocurrent (Fig. 2). This change was expected from the reduced absorption in the visible range (Fig. S4†). Despite this loss, the photocurrent density of two-component zipper Au-***r***-N-***R***-R already reached that of one-component zipper Au-***r***-R-***R***-R (Fig. 2A, Table 1, entry 4 *vs.* entry 1). Overall, the gain in photocurrent density per rNDI layer in zippers with an nNDI second layer was larger than that without nNDI layer (Fig. 2). This finding was compatible with the notion that the loss in absorption from a missing rNDI layer can be compensated by productively directing the flow of the produced electrons with nNDI acceptors toward the gold electrode. These findings thus were in support of operational two-component cascade π-stacks.

Three-component zippers

The behavior of three component zippers with rNDIs, nNDIs and bNDIs was more complex and subtle. Au-***r***-N-***R***-B, the simplest three-component zipper, had a very low $J_{SC} = 3.2\ \mu Acm^{-2}$ (Table 1, entry 7). This photocurrent density was not surprising considering the replacement of an excellent rNDI layer in Au-***r***-N-***R***-R ($J_{SC} = 11\ \mu Acm^{-2}$, Table 1, entry 4) with a poorly active terminal layer of bNDIs. The comparably poor photoactivity of bNDIs has been confirmed experimentally in the action spectra of two-component bNDI/rNDI zippers.[32] The inability of stack/rod electron transfer after absorption of light by bNDI, *i.e.*, the inability to form supramolecular n/p-heterojunctions, could contribute to this poor performance (Fig. 1). Alternative or additional explanations include poor electron transfer from the sacrificial TEOA donor to neutralize the hole trapped in the bNDI layer, or structural effects such as poor stacking of the less electron-deficient bNDIs.

The fill factor $FF = 0.38$ is surprisingly low considering the powerful productive asymmetry of the minimalist three-component zipper Au-***r***-N-***R***-B. The poor photoactivity of bNDIs may contribute to this reduction compared to the less asymmetric Au-***r***-N-***R***-R and Au-***r***-R-***R***-R (Table 1, entries 1, 4 and 7). Operational asymmetry in minimalist three-component zipper Au-***r***-N-***R***-B could nevertheless be demonstrated in comparison with the structural isomer Au-***r***-B-***R***-N with destructive asymmetry (Table 1, entries 7 and 13). In Au-***r***-B-***R***-N, the combination of unfavorable designs produced the worst zipper characteristics obtained so far with a $FF = 0.27$ that was equivalent to an almost linear IV profile (6% on a relative scale) and a very low V_{OC}. Addition of an rNDI layer on top improved photocurrents J_{SC} and FF but also obscured the differences with $FF = 0.47$ (or 61%) for Au-***r***-N-***R***-B-***R*** with favorable and $FF = 0.38$ (or 36%) for Au-***r***-B-***R***-N-***R*** with unfavorable asymmetry (Table 1, entries 8 and 14). This ability of rNDIs to improve zipper characteristics and obscure differences was even more pronounced on the next level with $FF = 0.54$ (or 81%) for the favorable Au-***r***-N-***R***-B-***R***-R and $FF = 0.48$ (or 64%) for Au-***r***-B-***R***-N-***R***-R with unfavorable asymmetry (Table 1, entries 9 and 15). $FF = 0.54$ (or 81%) for Au-***r***-N-***R***-B-***R***-R was the best fill factor found in this study, followed by $FF = 0.53$ (or 78%) for Au-***r***-N-***R***-R-***R***-R (Table 1, entries 9 and 3).

Increasing the distance between the nNDI electron acceptor and the bNDI electron donor had overall the expected consequences in zippers with favorable asymmetry. Moving the bNDI in the favorable Au-***r***-N-***R***-B-***R***-R to the film surface improved the photocurrent density to $J_{SC} = 11\ \mu Acm^{-2}$ in isomer Au-***r***-N-***R***-R-***R***-B (Table 1, entries 9 and 10). However, the best results were obtained with anionic bNDI propagators ***B*** rather than cationic bNDI propagators **B** near the surface. In the formal isomer Au-***r***-N-***R***-R-***B***-R, the photocurrent density improved to $J_{SC} = 12\ \mu Acm^{-2}$ and $FF = 0.51$ (or 72%) remained high (Table 1, entry 11). The same trend was already observed without the last cationic rNDI layer: The photocurrent density of Au-***r***-N-***R***-R-***B*** was 1.6-times higher than that of formal isomer Au-***r***-N-***R***-B-***R*** (Table 1, entries 8 and 12).

In zippers with unfavorable asymmetry, increasing the distance between the nNDI electron acceptor and the bNDI electron donor resulted in lowering of not only the photocurrent but also the fill factor from $FF = 0.48$ or 64% of Au-***r***-B-***R***-N-***R***-R to

Table 1 Short circuit current density J_{SC}, open circuit voltage V_{OC} and fill factor *FF* for one-, two-, and three-component zippers[a]

Entry		Zipper[b]	J_{SC}/μAcm^{-2}[c]	V_{OC}/V[d]	*FF*[e]
1	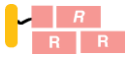	Au-***r***-**R**-***R***-**R**	12 (63)	–0.39	0.49 (67)
2		Au-***r***-**R**-***R***-**R**-***R***	15 (79)	–0.37	0.50 (69)
3	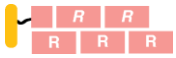	Au-***r***-**R**-***R***-**R**-***R***-**R**	17 (89)	–0.37	0.53 (78)
4	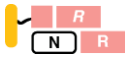	Au-***r***-**N**-***R***-**R**	11 (58)	–0.36	0.51 (72)
5	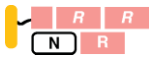	Au-***r***-**N**-***R***-**R**-***R***	15 (79)	–0.42	0.52 (75)
6	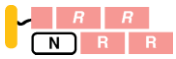	Au-***r***-**N**-***R***-**R**-***R***-**R**	19 (100)	–0.40	0.50 (69)
7	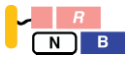	Au-***r***-**N**-***R***-**B**	3.2 (17)	–0.32	0.38 (36)
8	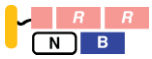	Au-***r***-**N**-***R***-**B**-***R***	5.8 (30)	–0.40	0.47 (61)
9	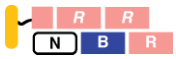	Au-***r***-**N**-***R***-**B**-***R***-**R**	9.3 (49)	–0.36	0.54 (81)
10	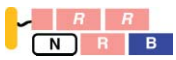	Au-***r***-**N**-***R***-**R**-***R***-**B**	11 (58)	–0.40	0.50 (69)
11	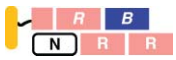	Au-***r***-**N**-***R***-**R**-***B***-**R**	12 (63)	–0.37	0.51 (72)
12	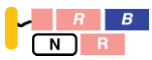	Au-***r***-**N**-***R***-**B**-***B***	9.4 (49)	–0.36	0.46 (58)
13	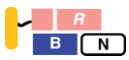	Au-***r***-**B**-***R***-**N**	3.3 (17)	–0.23	0.27 (6)
14	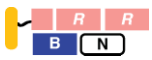	Au-***r***-**B**-***R***-**N**-***R***	4.7 (25)	–0.32	0.38 (36)
15	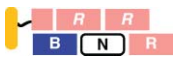	Au-***r***-**B**-***R***-**N**-***R***-**R**	13 (68)	–0.36	0.48 (64)
16	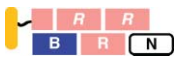	Au-***r***-**B**-***R***-**R**-***R***-**N**	8.7 (46)	–0.36	0.41 (44)
17	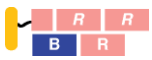	Au-***r***-**B**-***R***-**R**-***R***	15 (79)	–0.41	0.49 (67)
18	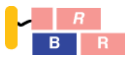	Au-***r***-**B**-***R***-**R**	14 (74)	–0.38	0.49 (67)

[a] Determined from current–voltage profiles (compare Fig. 3). [b] For molecular structures, see Fig. 1. [c] Short circuit current density; relative J_{SC} values in parentheses refer to a scale from 0 to 19 μAcm^{-2} (entry 6, in %). [d] Open circuit voltage (in volts). [e] Fill factors (*FF*) = maximum power/($V_{OC} \times J_{SC}$) = ($V_m \times J_m$)/($V_{OC} \times J_{SC}$) (compare Fig. 3); relative *FF* values in parentheses refer to a scale from 0.25 (minimum) to 0.61 (optimized organic solar cells,[1] in %). All experiments were done at least twice, experimental errors were within 10% (Fig. 2A).

FF = 0.41 or 44% of isomer Au-***r***-**B**-***R***-**R**-***R***-**N** (Table 1, entries 15 and 16). This decrease was reasonable considering the "wrong" location of the electron acceptor nNDI at the film surface. Unlike the other zippers, such as Au-***r***-**N**-***R***-**R**-***R***-**R** and Au-***r***-**N**-***R***-**R**-***R***-**B** (Fig. 2B, a and b), upon irradiation of isomer Au-***r***-**B**-***R***-**R**-***R***-**N** with unfavorable asymmetry the photocurrent increased very slowly, and saturated only after about 10 seconds (Fig. 2B, c). This phenomenon is unusual and illustrates very well the hindered uphill flow of electrons against the cascade NDI π-stack from nNDI acceptors to bNDI donors.

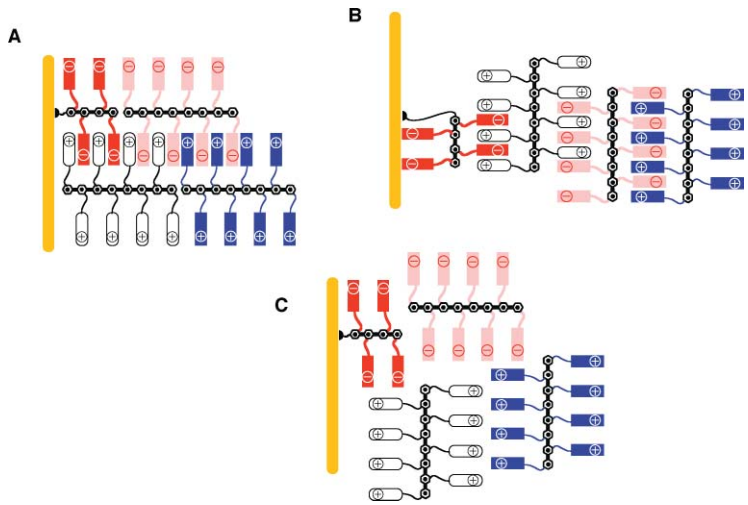

Fig. 4 Conceivable suprastructural motifs for minimalist three-component zippers Au-*r*-N-***R***-**B** include not only (A) "zippers" with inter- and intralayer interdigitation by rods and stacks but also (B) "horizontal" alternatives with interdigitating stacks or (C) less ordered layers without interdigitation of rods or stacks.

Conclusions

In this report, we demonstrate that multicomponent zipper assembly provides access to supramolecular rigid-rod π-stack cascade architectures with photovoltaic activity. The good correlation found between the expected supramolecular architectures and the measured photoactivity supports the existence of active architectures as drawn schematically in Fig. 1 and Fig. 4A. Although the comparison of data on structure and activity is much more problematic than it might appear,[55–57] we recall the availability of results in support of the proposed architecture (face-to-face NDI π-stacks supported by blue-shifted absorption, interdigitating rods supported by capping, *etc.*).[31] However, these results do not exclude functional relevance of suprastructures other than the envisioned zipper assembly (*e.g.*, Fig. 4B, and Fig. 4C), not to speak of other possible contributions to the final phenotype (minor or major differences in binding to the surface, layer thickness, layer homogeneity, suprastructural homogeneity, and so on).

In a broader context, the complex interplay of experimental details such as choice of solvents, solvent mixtures, concentrations, temperature, pH, ionic strength, additives processing conditions, thermal or chemical annealing and the choice of electrodes and donors/acceptors in solution are as well recognized as they are poorly understood. For example, change of solvent or thermal annealing significantly changes efficiency and fill factors of conventional bulk heterojunction solar cells.[1,58] The change from gold to ITO (indium tin oxide) electrodes can improve photocurrent generation by a factor of 280.[59] Whereas gold is the substrate of choice to determine the importance of multicomponent cascade architectures for function, it is therefore inadequate to aim for meaningful efficiencies. These observations indicate that the reported facts on function for up to three-component zipper assembly have to be considered as relative and within an appropriate context.

As far as perspectives are concerned, the possibility to expand multicomponent zipper assembly to include several NDIs[45–49] as variable electron/energy donors/acceptors of variable color in variable patterns promises access to the complexity associated with interesting function. Elaboration of structural diversity covering other rods, stacks, surfaces and interactions is expected to ultimately delineate scope and limitations of this general approach.

Acknowledgements

We thank S. Bhosale, A. L. Sisson and D.-H. Tran for contributions to synthesis, D. Jeannerat, A. Pinto and S. Grass for NMR measurements, P. Perrottet and the group of F. Gülaçar, N. Oudry and G. Hopfgartner for MS, and the University of Geneva and the Swiss NSF and for financial support.

References

1 B. C. Thompson and J. M. J. Fréchet, *Angew. Chem., Int. Ed.*, 2008, **47**, 58–77.
2 V. Balzani, M. Venturi and A. Credi, *Molecular Devices and Machines*, Wiley-VCH, Weinheim, 2003.
3 M. Grätzel, *Pure Appl. Chem.*, 2001, **73**, 459–467.
4 J.-F. Eckert, J.-F. Nicoud, J.-F. Nierengarten, S.-G. Liu, L. Echegoyen, N. Armaroli, F. Barigelletti, L. Ouali, V. Krasnikov and G. Hadziioannou, *J. Am. Chem. Soc.*, 2000, **122**, 7467–7479.
5 G. Yu, J. Gao, J. C. Hummelen, F. Wudl and A. J. Heeger, *Science*, 1995, **270**, 1789–1791.
6 E. A. Weiss, V. J. Porter, R. C. Chiechi, S. M. Geyer, D. C. Bell, M. G. Bawendi and G. M. Whitesides, *J. Am. Chem. Soc.*, 2008, **130**, 83–92.
7 A. Kongkanand, K. Tvrdy, K. Takechi, M. Kuno and P. V. Kamat, *J. Am. Chem. Soc.*, 2008, **130**, 4007–4015.
8 F. Würthner, Z. Chen, F. J. M. Hoeben, P. Osswald, C.-C. You, P. Jonkheijm, J. Herrikhuyzen, A. P. H. J. Schenning, P. P. A. M. van der Schoot, E. W. Meijer, E. H. A. Beckers, S. C. J. Meskers and R. A. J. Janssen, *J. Am. Chem. Soc.*, 2004, **126**, 10611–10618.
9 Y. Yamamoto, T. Fukushima, Y. Suna, N. Ishii, A. Saeki, S. Seki, S. Tagawa, M. Taniguchi, T. Kawai and T. Aida, *Science*, 2006, **314**, 1761–1764.
10 S. Kang, T. Umeyama, M. Ueda, Y. Matano, H. Hotta, K. Yoshida, S. Isoda, M. Shiro and H. Imahori, *Adv. Mater.*, 2006, **18**, 2549–2552.
11 R. A. Miller, A. D. Presley and M. B. Francis, *J. Am. Chem. Soc.*, 2007, **129**, 3104–3109.
12 R. Koeppe, O. Bossart, G. Calzaferri and N. S. Sariciftci, *Sol. Energy Mater. Sol. Cells*, 2007, **91**, 986–995.
13 J. C. Love, L. A. Estroff, J. K. Kriebel, R. G. Nuzzo and G. M. Whitesides, *Chem. Rev.*, 2005, **105**, 1103–1169.

14 T. Kondo and K. Uosaki, *J. Photochem. Photobiol. C: Photochem. Rev.*, 2007, **8**, 1–17.
15 S. Kimura, *Org. Biomol. Chem.*, 2008, **6**, 1143–1148.
16 I. Carmeli, L. Frolov, C. Carmeli and S. Richter, *J. Am. Chem. Soc.*, 2007, **129**, 12352–12353.
17 T. Takada, C. Lin and T. Majima, *Angew. Chem., Int. Ed.*, 2007, **46**, 6681–6683.
18 H. Imahori, Y. Mori and Y. Matano, *J. Photochem. Photobiol. C: Photochem. Rev.*, 2003, **4**, 51–83.
19 S. Fukuzumi, *Bull. Chem. Soc. Jpn.*, 2006, **79**, 177–195.
20 G. Decher, *Science*, 1997, **277**, 1232–1237.
21 J. K. Mwaura, M. R. Pinto, D. Witker, N. Ananthakrishnan, K. S. Schanze and J. R. Reynolds, *Langmuir*, 2005, **21**, 10119–10126.
22 T. Fushimi, A. Oda, H. Ohkita and S. Ito, *Langmuir*, 2005, **21**, 1584–1589.
23 H. Li, Y. Li, J. Zhai, G. Cui, H. Liu, S. Xiao, Y. Liu, F. Lu, L. Jiang and D. Zhu, *Chem.–Eur. J.*, 2003, **9**, 6031–6038.
24 M. Lahav, V. Heleg-Shabtai, J. Wasserman, E. Katz, I. Willner, H. Dürr, Y.-Z. Hu and S. H. Bossmann, *J. Am. Chem. Soc.*, 2000, **122**, 11480–11487.
25 D. M. Guldi, *J. Phys. Chem. B*, 2005, **109**, 11432–11441.
26 A. Ikeda, T. Hatano, S. Shinkai, T. Akiyama and S. Yamada, *J. Am. Chem. Soc.*, 2001, **123**, 4855–4856.
27 C.-H. Huang, N. D. McClenaghan, A. Kuhn, G. Bravic and D. M. Bassani, *Tetrahedron*, 2006, **62**, 2050–2059.
28 M. Morisue, S. Yamatsu, N. Haruta and Y. Kobuke, *Chem.–Eur. J.*, 2005, **11**, 5563–5574.
29 F. B. Abdelrazzaq, R. C. Kwong and M. E. Thompson, *J. Am. Chem. Soc.*, 2002, **124**, 4796–4803.
30 A. B. F. Martinson, A. M. Massari, S. J. Lee, R. W. Gurney, K. E. Splan, J. T. Hupp and S. T. Nguyen, *J. Electrochem. Soc.*, 2006, **153**, A527–A532.
31 N. Sakai, A. L. Sisson, T. Bürgi and S. Matile, *J. Am. Chem. Soc.*, 2007, **129**, 15758–15759.
32 A. L. Sisson, N. Sakai, N. Banerji, A. Fürstenberg, E. Vauthey and S. Matile, *Angew. Chem., Int. Ed.*, 2008, **47**, 3727–3729.
33 G. Das and S. Matile, *Chirality*, 2001, **13**, 170–176.
34 N. Sakai, J. Mareda and S. Matile, *Acc. Chem. Res.*, 2005, **38**, 79–87.
35 P. Talukdar, G. Bollot, J. Mareda, N. Sakai and S. Matile, *J. Am. Chem. Soc.*, 2005, **127**, 6528–6529.
36 S. Bhosale, A. L. Sisson, P. Talukdar, A. Fürstenberg, N. Banerji, E. Vauthey, G. Bollot, J. Mareda, C. Röger, F. Würthner, N. Sakai and S. Matile, *Science*, 2006, **313**, 84–86.
37 S. Bhosale, A. L. Sisson, N. Sakai and S. Matile, *Org. Biomol. Chem.*, 2006, **4**, 3031–3039.
38 S. V. Bhosale, C. H. Jani and S. J. Langford, *Chem. Soc. Rev.*, 2008, **37**, 331–342.
39 R. S. Lokey and B. L. Iverson, *Nature*, 1995, **375**, 303–305.
40 L. L. Miller and K. R. Mann, *Acc. Chem. Res.*, 1996, **29**, 417–423.
41 H. E. Katz, A. J. Lovinger, J. Johnson, C. Kloc, T. Siegrist, W. Li, Y. Y. Lin and A. Dodabalapur, *Nature*, 2000, **404**, 478–481.
42 T. Iijima, S. A. Vignon, H. R. Tseng, T. Jarrosson, J. K. M. Sanders, F. Marchioni, M. Venturi, E. Apostoli, V. Balzani and J. F. Stoddart, *Chem.–Eur. J.*, 2004, **10**, 6375–6392.
43 P. Mukhopadhyay, Y. Iwashita, M. Shirakawa, S. Kawano, N. Fujita and S. Shinkai, *Angew. Chem., Int. Ed.*, 2006, **45**, 1592–1595.
44 A. Morandeira, J. Fortage, T. Edvinsson, L. Le Pleux, E. Blart, G. Boschloo, A. Hagfeldt, L. Hammarström and F. Odobel, *J. Phys. Chem. C*, 2008, **112**, 1721–1728.
45 B. A. Jones, A. Facchetti, M. R. Wasielewski and T. J. Marks, *J. Am. Chem. Soc.*, 2007, **129**, 15259–15278.
46 F. Würthner, S. Ahmed, C. Thalacker and T. Debaerdemaeker, *Chem.–Eur. J.*, 2002, **8**, 4742–4750.
47 C. Thalacker, C. Röger and F. Würthner, *J. Org. Chem.*, 2006, **71**, 8098–8105.
48 C. Röger and F. Würthner, *J. Org. Chem.*, 2007, **72**, 8070–8075.
49 A. Blaszczyk, M. Fischer, C. von Hänisch and M. Mayor, *Helv. Chim. Acta*, 2006, **89**, 1986–2005.
50 V. Gorteau, G. Bollot, J. Mareda, A. Perez-Velasco and S. Matile, *J. Am. Chem. Soc.*, 2006, **128**, 14788–14789.
51 V. Gorteau, G. Bollot, J. Mareda and S. Matile, *Org. Biomol. Chem.*, 2007, **5**, 3000–3012.
52 H. Tanaka, G. Bollot, J. Mareda, S. Litvinchuk, D.-H. Tran, N. Sakai and S. Matile, *Org. Biomol. Chem.*, 2007, **5**, 1369–1380.
53 S. Hagihara, H. Tanaka and S. Matile, *J. Am. Chem. Soc.*, 2008, **130**, 5656–5657.
54 N. Banerji, A. Fürstenberg, S. Bhosale, A. L. Sisson, N. Sakai, S. Matile and E. Vauthey, *J. Phys. Chem. B*, 2008, **112**, 8912–8922.
55 A. R. Murphy and J. M. J. Fréchet, *Chem. Rev.*, 2007, **107**, 1066–1096.
56 A. Perez-Velasco, V. Gorteau and S. Matile, *Angew. Chem., Int. Ed.*, 2008, **47**, 921–923.
57 S. Bhosale and S. Matile, *Chirality*, 2006, **18**, 849–856.
58 X. Yang, J. Loos, S. C. Veenstra, W. J. H. Verhees, M. M. Wienk, J. M. Kroon, M. A. J. Michels and R. A. J. Janssen, *Nano Lett.*, 2005, **5**, 579–583.
59 H. Yamada, H. Imahori, Y. Nishimura, I. Yamazaki, T. K. Ahn, S. K. Kim, D. Kim and S. Fukuzumi, *J. Am. Chem. Soc.*, 2003, **125**, 9129–9139.

